





Article

Solubility of Rosmarinic Acid in Supercritical Carbon Dioxide Extraction from *Orthosiphon stamineus* Leaves

Ahmad Hazim Abdul Aziz ^{1,*}, Nor Faadila Mohd Idrus ², Nicky Rahmana Putra ², Mohd Azrie Awang ¹, Zuhaili Idham ², Hasmadi Mamat ¹ and Mohd Azizi Che Yunus ²

¹ Faculty of Food Science and Nutrition, Universiti Malaysia Sabah, Kota Kinabalu 88400, Malaysia; ma.awang@ums.edu.my (M.A.A.); idamsah@ums.edu.my (H.M.)

² School of Chemical and Energy Engineering, Faculty of Engineering, Universiti Teknologi Malaysia, Johor Bahru 81310, Malaysia; faadilaidrus@gmail.com (N.F.M.I.); nickyrahman1309@gmail.com (N.R.P.); zuhailiidham@utm.my (Z.I.); azizi@cheme.utm.my (M.A.C.Y.)

* Correspondence: hazim.aziz@ums.edu.my

Abstract: Rosmarinic acid (RA) is present in a broad variety of plants, including those in the Lamiaceae family, and has a wide range of pharmacological effects, particularly antioxidant activity. To extract RA from *Orthosiphon stamineus* (OS) leaves, a Lamiaceae plant, a suitable extraction process is necessary. The present study used a green extraction method of supercritical carbon dioxide (SCCO₂) extraction with the addition of ethanol as a modifier to objectively measure and correlate the solubility of RA from OS leaves. The solubility of RA in SCCO₂ was determined using a dynamic extraction approach, and the solubility data were correlated using three density-based semi-empirical models developed by Chrastil, del Valle-Aguilera, and Gonzalez. Temperatures of 40, 60, and 80 °C and pressures of 10, 20, and 30 MPa were used in the experiments. The maximum RA solubility was found at 80 °C and 10 MPa with 2.004 mg of rosmarinic acid/L solvent. The RA solubility data correlated strongly with the three semi-empirical models with less than 10% AARD. Furthermore, the fastest RA extraction rate of 0.0061 mg/g min⁻¹ was recorded at 80 °C and 10 MPa, and the correlation using the Patricelli model was in strong agreement with experimental results with less than 15% AARD.

Keywords: solubility; extraction rate; supercritical carbon dioxide extraction; *Orthosiphon stamineus*; rosmarinic acid



Citation: Abdul Aziz, A.H.; Mohd Idrus, N.F.; Putra, N.R.; Awang, M.A.; Idham, Z.; Mamat, H.; Che Yunus, M.A. Solubility of Rosmarinic Acid in Supercritical Carbon Dioxide Extraction from *Orthosiphon stamineus* Leaves. *ChemEngineering* **2022**, *6*, 59. <https://doi.org/10.3390/chemengineering6040059>

Academic Editor: Roumiana Petrova Stateva

Received: 28 June 2022

Accepted: 19 July 2022

Published: 1 August 2022

Publisher's Note: MDPI stays neutral with regard to jurisdictional claims in published maps and institutional affiliations.



Copyright: © 2022 by the authors. Licensee MDPI, Basel, Switzerland. This article is an open access article distributed under the terms and conditions of the Creative Commons Attribution (CC BY) license (<https://creativecommons.org/licenses/by/4.0/>).

1. Introduction

Orthosiphon stamineus (OS) is a Lamiaceae family medicinal herb also known as “cat’s whiskers” or “misai kucing” that is commonly found in Southeast Asian nations such as the Philippines, Malaysia, Brunei, Thailand, and Indonesia. For several decades, the leaves have been widely consumed in the form of tea, also known as Java tea, to treat a variety of harmful diseases such as gonorrhea, diabetes, hypertension, tonsillitis, syphilis, gallstones, gout arthritis, and kidney stones [1–4]. The plant contains essential oil with α -humulene, limonene, β -caryophyllene, and others, diterpenes (0.2–0.3%) with orthosiphols, orthosiphonones, staminols, and others, flavonoids (0.4–0.5%) with sinensetin, isosinensetin, eupatorine, salvigenin, and others, phenolic acids (0.5–1.0%) with rosmarinic acid, caffeic acid, cichoric acid, and others, triterpenes with ursolic acid, betulinic acid, and others, chromenes, and others [5]. There have been numerous studies conducted to date to investigate the medicinal benefits of OS leaves. It is reported that the OS leaves have a variety of pharmacological properties such as antioxidant, anti-inflammatory, antibacterial, diuretic, antidiabetic, antimicrobial, antitumor, antimutagenic, antiproliferative, and antihypertensive properties [6–11]. OS is currently in high demand in the herbal and pharmaceutical industries due to its medicinal [12] and economic value [13].

Rosmarinic acid (RA) is caffeic acid and 3,4-dihydroxyphenyl lactic acid ester found in a variety of Lamiaceae species including lemon balm, peppermint, oregano, rosemary, sage,

and thyme [14–16]. It is naturally synthesized in plants via the shikimate/phenylpropanoid pathway [17]. Caffeic acid ester compounds have poor lipophilicity and inhibit intracellular entrance. According to Akowuah and Zhari [18] and Abdul Aziz [19], RA is a major polyphenol found in OS leaves. Among phenolic compounds, RA is structurally interesting due to its strong natural antioxidant [20] and its variety of effects such as anti-inflammatory, antibacterial, antiviral, antidiabetic, and antiallergic properties [21,22]. Shekarchi [23] reported that RA has greater antioxidant activity than vitamin E. Because of these benefits, RA is frequently employed in the food, cosmetics, and pharmaceutical industries [24]. As a result, the demand for RA has skyrocketed, spurring the development of efficient extraction technologies from its natural sources, particularly OS leaves.

Supercritical carbon dioxide (SCCO₂) extraction has been widely explored for the extraction of polyphenols such as rosmarinic acid, squalene, catechin, lycopene, and others from diverse plant-derived matrices and has been proven to be a promising technology [25–28]. SCCO₂ extraction has a mild critical temperature, T_c of 31.1 °C, and a critical pressure, P_c of 7.38 MPa. A moderate extraction temperature of 40 to 80 °C may be helpful in avoiding thermal damage when isolating a high-purity bioactive compound. By adjusting the extraction parameters of temperature and pressure, SCCO₂ has outstanding properties such as high density, high dissolving power, high diffusivity, low surface tension, and low viscosity [28,29]. Furthermore, SCCO₂ facilitates the process of separating the extract by depressurizing it, resulting in a solvent-free extract. Due to these advantages, SCCO₂ extraction is highly valued in replacing the organic solvents in traditional extraction processes.

The concentration of RA extracted using SCCO₂ from dragonhead (*Dracocephalum moldavica*) seed was reported to be approximately 1.20 mg/g [30]. Meanwhile, Bakota [31] extracted 28.4 mg RA/g from sage (*Salvia officinalis*) leaves at 80 °C and 55.2 MPa. In contrast, Lefebvre [32] reported that RA from rosemary was not extracted in pure SCCO₂, but with the addition of 10% ethanol yielded approximately 78 mg/g of RA. Al-Suede [4] discovered a similar pattern in which RA is not present in the SCCO₂ extract yield of OS leaves. This is due to the fact that RA is a hydrophilic or polar compound that has a strong attraction to water or polar solvent molecules. Meanwhile, CO₂ is a non-polar solvent and has a disadvantage in extracting polar compounds. Thus, adding a small amount of co-solvent or modifier to SCCO₂ can significantly improve both its solvent power and polarity. Modifiers that are commonly used include benzene, methylene chloride, petroleum ether, hexane, acetone, methanol, ethanol, toluene, and water as typical co-solvents [33–35]. Because of the hazardous nature of most organic solvents and the concomitant challenge of completely eliminating modifier residue from processed material, the function of a modifier has been limited in the food and pharmaceutical industries. Furthermore, the presence of a modifier in SCCO₂ may increase solute melting point depressivity, which is associated with a reduction in the system's upper critical endpoint pressure [36]. Dipole–dipole interactions and hydrogen bonds created between the solute and the modifier significantly increase the solute's solubility, according to Huang [37] and Bitencourt [38]. Therefore, ethanol is a polar solvent in nature due to the presence of a hydroxyl group and has been authorized in food industries due to being less harmful than other organic solvents [39,40]. As a consequence, our earlier investigation of OS leaves extraction using SCCO₂-assisted ethanol revealed that the concentration of RA is greatest at 931.44 mg/kg, followed by sinensetin and isosinensetin at 469.54 and 419.07 mg/kg, respectively [19].

A thorough understanding of solubility data and compound behavior in SCCO₂ is essential for determining the feasibility of supercritical separation of the target compound and defining suitable operating conditions. The correct information about the solute solubility is required for the successful application of SCCO₂ [41]. Therefore, much research has sought to offer information on the solubility of various bioactive compounds in SCCO₂ [41–46]. To date, there have been no published studies on the solubility of RA in the SCCO₂ system. There are numerous ways to determine the solubility of a compound in SCCO₂. A dynamic approach is the most commonly used by researchers to calculate solubility. This

method has been proven to be effective since it allows for the collection of a large number of fractionation data in a short amount of time. However, because acquiring equilibrium or solubility data at high temperatures and pressures is tedious and expensive, predictive models are critical.

Various mathematical models have been established, including the equation of state (EOS) and semi-empirical models. Because thermodynamic data are limited, the latter is significantly more recommended and favored. Rosales-García [47] observed squalene solubility in SCCO₂ at various temperatures and pressures. They also used a number of semi-empirical models with an average absolute relative deviation of less than 10% (AARD%) to predict the measured solubility data. In another work, the solubility of cinnamic acid in SCCO₂ was obtained via a dynamic approach at various temperatures and pressures [48]. The authors used 10 density-based semi-empirical models of Chrastil [49], Adachi-Lu [50], Kumar-Johnston [51], Sung-Shim [52], Mendez-Santiago-Teja [53], Bartle [54], Gonzalez [55], Sovova [56], Tang [57], and Sauceau [58]. They reported that these models showed great agreement with the experimental data for less than 10% of AARD. Zhan [59], Jin [60], Wei [61], and Jia [62] showed that several semi-empirical models were the most accurate in forecasting compound solubility in SCCO₂ with the lowest AARD%. This is due to the fact that these models have the benefit of fitting all experimental data for each solute with as few as three to six parameters. These models are also beneficial for data correlations and testing the model fit due to their simplicity, as previously reported [63].

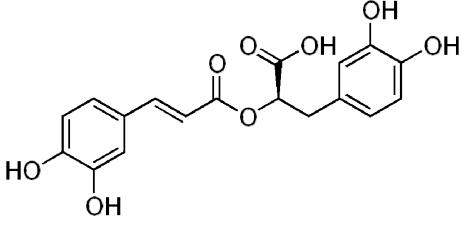
For the first time, the solubility data of RA in assisted-ethanol SCCO₂ systems at varied temperatures (40, 60, and 80 °C) and pressures (10, 20, and 30 MPa) were correlated using three well-known density-based semi-empirical models of Chrastil, del Valle-Aguilera (dVA), and Gonzalez. The versatility of these models in terms of the number of configurable parameters and their capacity to predict thermodynamic parameters such as total enthalpy, enthalpy of vaporization, and enthalpy of solvation were the primary reasons for their consideration. Furthermore, the influence of co-solvent in the system can be evaluated. The semi-empirical models are widely used in the previous study due to its accuracy in correlating with solubility data in the SCCO₂ extraction process. In addition, the mass transfer coefficient and RA extraction rate in the ethanol-assisted SCCO₂ system were calculated concurrently using the Patricelli model.

2. Materials and Methods

2.1. Chemicals and Materials

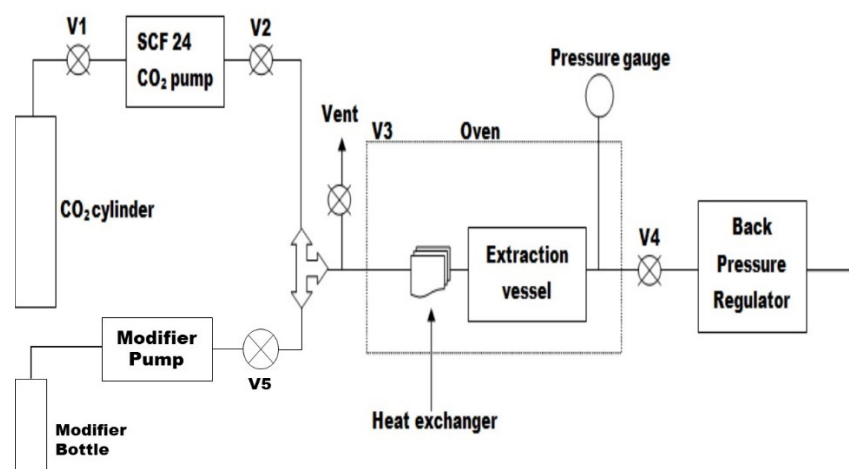
All of the chemicals and reagents were analytical reagent grade. Kras Instrument and Services (Johor, Malaysia) supplied 99.99% pure carbon dioxide. Sigma-Aldrich, Darmstadt, Germany, provided the RA reference standard. The physical properties of RA were predicted using the group contribution method generated from the ICAS 17 software and are listed in Table 1. Analytical-grade ethanol, acetonitrile, isopropyl alcohol, orthophosphoric acid, and sodium dihydrogen phosphate anhydrous phosphate buffer were utilized. Dry OS aerial parts were provided by Bioalpha Holdings Berhad (Selangor, Malaysia). The leaves were segregated from the aerial part and triturated to a mean particle size of 400 to 500 µm. To avoid contamination, the ground samples were packed and stored in a refrigerator at −20 °C [64].

Table 1. Properties of rosmarinic acid.

Properties	Rosmarinic Acid
Chemical Structure	
Formula	C ₁₈ H ₁₆ O ₈
Molecular weight	360.31 g/mol
Melting point	231.38 °C
Boiling point	495.29 °C
Critical temperature	678.26 °C
Critical pressure	4.427 MPa
Molar Volume	250.79 cm ³ /mol
Solubility parameter	35.02 MPa ^{1/2}
Dipole moment	5.3023 Debye

2.2. Supercritical Carbon Dioxide (SCCO₂) Extraction

SCCO₂ extraction at the laboratory scale was carried out at temperatures and pressures of 40, 60, and 80 °C and 10, 20, and 30 MPa, respectively, using ethanol as a modifier. Figure 1 depicts a schematic diagram of the extraction process based on previous work [19,65,66]. The apparatus setup consists of a carbon dioxide (CO₂) tank, a circulating water bath (WiseCircu), a CO₂ pump (Lab Alliance, Supercritical 24: Constant flow with dual-piston pump), a pressure gauge, an oven with a 10 mL extraction vessel, and a back pressure regulator (BPR) (Jasco, Model BP-2080, Pfungstadt, Germany) with a restrictor valve. For a modifier, a 10 mL Series II pump (Scientific Systems, Inc., Woburn, MA, USA) was employed. The tubing system used was 1/16 inches in diameter. The temperature of the process was set in the extraction chamber or oven and pressure was controlled by BPR. The restrictor valve released the pressure when the system achieved the desired pressure by depressurization.

**Figure 1.** Schematic diagram of SCCO₂ extraction with modifier.

2.3. Quantification of RA

The amount of RA extracted from OS leaves was measured using High-Performance Liquid Chromatography (HPLC). The complete analysis approach has also been previously disclosed here [19]. A calibration curve was used to examine the quantification of bioactive chemicals by graphing standard concentrations of the standards (20, 40, 60, 80, and 100 ppm) vs. its peak areas. The RA standard curve is $Y = 55.3X$, with a regression correlation (R^2) of 0.995 and a retention duration of 1.859 min.

2.4. Solubility Measurement and Correlation

A dynamic extraction method was used to extract RA from OS leaves. The initial slope of the extraction curve known as the constant extraction rate (CER) phase on the graph of solute concentration vs. solvent used was used to calculate the experimental solute solubility. To anticipate the solubility behavior of RA in SCCO_2 , three density-based semi-empirical models were utilized to correlate the experimental solubility data. Chrastil [49] was the first to use the system's density and temperature to develop a semi-empirical model that correlates solids' and liquids' solubility in supercritical gases (binary system), as described below:

$$\ln S = k \ln \rho_{mix} + \frac{a}{T} + b \quad (1)$$

where S (g/L) is the compound's solubility, k is an association coefficient, ρ_{mix} (g/L) is the density of the solvent mixture, and T (K) is the temperature. Constant a is an adjustable parameter that incorporates the total heat of the reaction. In contrast, constant b is an adjustable parameter that relates to the association number and molar masses of the solute and solvent.

The del Valle and Aguilera [67] (dVA) model expanded on Chrastil's by including one more parameter that connects the temperature to the solute solubility in quadratic form, as indicated in the equation below:

$$\ln S = k \ln \rho_{mix} + \frac{a}{T} + \frac{b}{T^2} + c \quad (2)$$

where constants a and b indicate the temperature effect involved in the solubilization process, while constant c represents the molecular weight of the solute and solvent. We refer readers to our previous work to calculate the density of the solvent mixture [64].

Gozález [55], on the other hand, adapted the Chrastil model to account for the formation of compound-modifier complexes in the presence of the modifier (ternary system), as illustrated below:

$$\ln S = k \ln \rho + \gamma \ln c + \frac{a}{T} + b \quad (3)$$

where γ is the modifier's association number and c is its concentration.

2.5. Extraction Rate

The Patricelli method was used to calculate the rate of RA extraction in the SCCO_2 extraction. In a Patricelli model, the extraction curve is governed by two-phase boundaries known as washing and diffusion. Solutes dissolve into the solvent via a damaged cell wall with minimal mass transfer resistance during the washing phase. Meanwhile, during the diffusion phase, solutes from the interior cell wall diffuse into the solvent. The Patricelli model [68] was then stated as the following equation:

$$C_{RA} = C_w(1 - \exp(-k_w t)) + C_d(1 - \exp(-k_d t)) \quad (4)$$

where C_w (mg/g) is the solute equilibrium concentration during washing, C_d (mg/g) is the solute equilibrium concentration during the diffusion, k_w and k_d (min^{-1}) are the mass

transfer coefficients during the washing and diffusion phases, respectively, and t (min) is the extraction time. The extraction rate is therefore shown as in Equation (5):

$$R_t = k_w C_w + k_d C_d \quad (5)$$

2.6. Validation

Non-linear regression data fits were evaluated using a Microsoft Excel 2019 (Redmond, WA, USA) with Solver tool. As mentioned in Equation (6), the best-fitting models will look at the percentage of average absolute relative deviation (AARD%):

$$AARD, \% = \frac{1}{n} \sum_{i=1}^n \left| \frac{N_{exp} - N_{calc}}{N_{exp}} \right| \times 100\% \quad (6)$$

where n is a number of data points, N_{exp} is the value of the experiments, and N_{calc} is the calculated value from the models.

3. Results and Discussion

3.1. Solubility of RA in the SCCO₂ System

Dynamically, the solubility of RA from OS leaves in ethanol-assisted SCCO₂ was investigated utilizing the CER gradient at temperatures ranging from 40 to 80 °C and pressures ranging from 10 to 30 MPa. The solubility of RA was changed from 0.056 to 2.004 mg/L solvent, as indicated in Table 2. The highest RA solubility was obtained at 80 °C and 10 MPa, which corresponded to the lowest density at 229.611 g/L, whereas the lowest RA solubility was obtained at 40 °C and 20 MPa, which corresponded to a greater density of 836.246 g/L.

Table 2. Solubility data of RA at various temperatures and pressures.

Temperature (°C)	Pressure (MPa)	Density (g/L)	Experimental RA Solubility (mg/L solvent)	Predicted RA Solubility (mg/L)
40	10	634.603	0.385	0.282
40	20	836.246	0.056	0.212
40	30	901.966	0.144	0.196
60	10	299.201	0.677	0.677
60	20	725.224	0.192	0.271
60	30	825.800	0.251	0.237
80	10	229.611	2.004	0.970
80	20	599.789	0.174	0.360
80	30	745.349	0.306	0.288

Table 2 demonstrates that as pressure increases from 10 MPa to 20 MPa at each isotherm, RA solubility is reduced while it increases to 30 MPa as the RA solubility increases. These phenomena occur when pressure increases, causing the solvent's ability to extract more polar molecules, while becoming less selective and extracting more by-products. Increasing the pressure generally raises the density of SCCO₂, which improves its solvating power before boosting the extraction process and solubility. As pressure increases, however, diffusivity falls as viscosity increases [69]. The solvent molecules are unable to dissolve the solute because they are difficult to disperse into pores. Furthermore, raising the SCCO₂ pressure results in a more robust solid matrix, reducing both the void fraction and the extraction efficiency. The pressure increases from 10 to 30 MPa caused competing influences, leading to a change in the RA solubility data.

The improved RA solubility at higher extraction temperatures should aid in both the breaking of hard structures and the desorption of RA bound to the plant matrix, as well as increasing the rate of solute diffusion out of the matrix pores into the supercritical bulk flow. The greater the density, however, the greater the solvating power of SCCO₂ can be obtained by increasing the pressure. Indeed, as pressure increases, the compactness of the molecules increases, resulting in higher density and more solvent solvating power.

In general, supercritical fluid density and solute vapor pressure are two important parameters that influence solute solubility in the supercritical fluid system. Temperature has two contradictory effects: The first is a reduction in density as the temperature rises, and the second is a change in solid sublimation pressure or solute vapor pressure, which can have an increasing influence on the solubility in the SCCO₂. As a result, there may be a net influence of these two competing effects (occurring throughout all temperature ranges) indicating that temperature has an increasing or reducing effect on the solute solubility. The solubility of RA, on the other hand, displays an increasing effect only when the temperature is increased from 40 to 80 °C at isobaric conditions ranging from 10 to 30 MPa.

3.2. Solubility Correlation of RA in SCCO₂ System

Chrastil, dVA, and Gonzalez models were used to correlate RA solubility data. Table 3 lists the density-based semi-empirical model constants as well as AARD. It can be seen from there that the AARD values (%) of the three models range from 5.184 to 8.566%. All models demonstrated a strong correlation with experimental data on RA solubility. The dVA model provides the lowest AARD (%) value for RA solubility, followed by the Chrastil and Gonzalez models.

Table 3. Correlations results of the solubility of RA by semi-empirical models.

Models	Model Parameters	Model Coefficient
Chrastil	k	−1.012
	a	−446.398
	b	−0.187
	AARD (%)	5.245
dVA	k	−1.033
	a	−391.280
	b	−19,889.733
	c	−0.057
	AARD (%)	5.184
Gonzalez	k	−0.100
	γ	−0.888
	a	−576.936
	b	7.193×10^{-4}
	AARD (%)	8.566

The negative sign of k indicated that increasing the system pressure could reduce the solubility of RA. Meanwhile, Chrastil and dVA models were able to calculate the thermodynamic enthalpy (ΔH_t , ΔH_v , and ΔH_s). Constant *a* in the Chrastil equation, where $a = (\Delta H_t)/R$ and *R* is the gas constant ($8.314 \text{ J mol}^{-1}\text{K}^{-1}$), was used to calculate the value of ΔH_t for RA, which was 3.711 kJ/mol. Meanwhile, the del Valle–Aguilera model could calculate the enthalpy of vaporization for RA ($\Delta H_v(T) = R(a + 2b/T)$) at 4.309 kJ/mol [63]. As a result, subtracting ΔH_v from ΔH_t yielded a value of enthalpy of sublimation for RA (ΔH_s) of approximately −0.598 kJ/mol. Our findings are consistent with our previous work [64], which concluded that vaporization is an endothermic process while solvation is exothermic. The Gonzalez model, on the other hand, reveals that ethanol has a considerable effect on the solubility of RA ($\gamma > k$). Table 2 shows that the prediction solubility values have a high correlation (R^2) with the experimental data of RA of approximately 0.938.

In comparison to other bioactive components from OS, such as sinensetin and isosinensetin, the solubility of RA is lowest in our earlier work on Abdul Aziz [64]. The presence of four hydroxyl groups (−OH) in the RA structure, which formed hydrogen bonds between

its molecules, explains this occurrence. The RA solute–solute interactions were optimized with Gaussian version 09 software (Gaussian, Inc., Wallingford, CT, USA) utilizing density functional theory (DFT) at the B3LYP level of theory and the 6-311G (d,p) basis set (Figure 2). As a result, the carboxyl group (-COOH) in the RA structure resulted in greater RA solute–solute interactions, with an intermolecular distance of 1.669 Å. This leads to the formation of dimerization, which creates a steric hindrance. The intermolecular distances of sinensetin and isosinensetin were reported to be approximately 2.454 Å and 2.395 Å, respectively, implying that the solubility of sinensetin and isosinensetin is higher than RA. Because there is no hydrogen bonding in the structure, dipoles–dipoles interactions are weaker than hydrogen bonds.

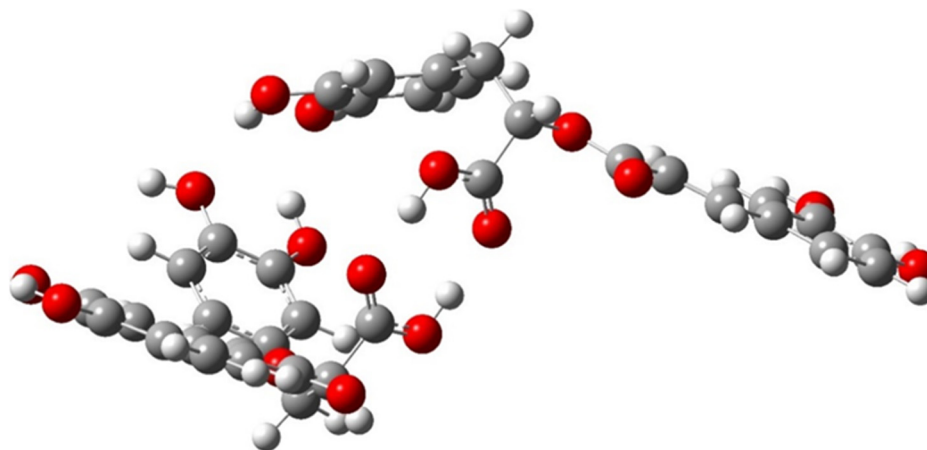


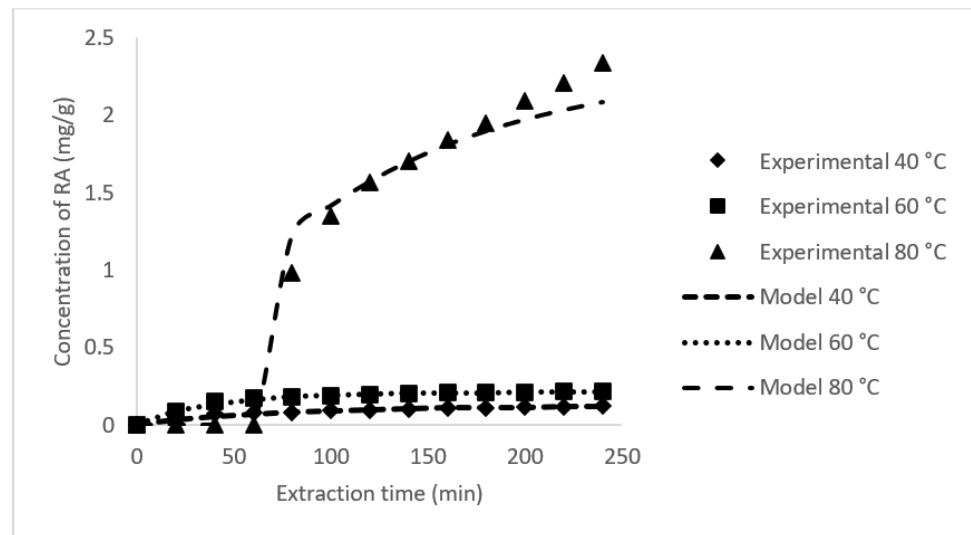
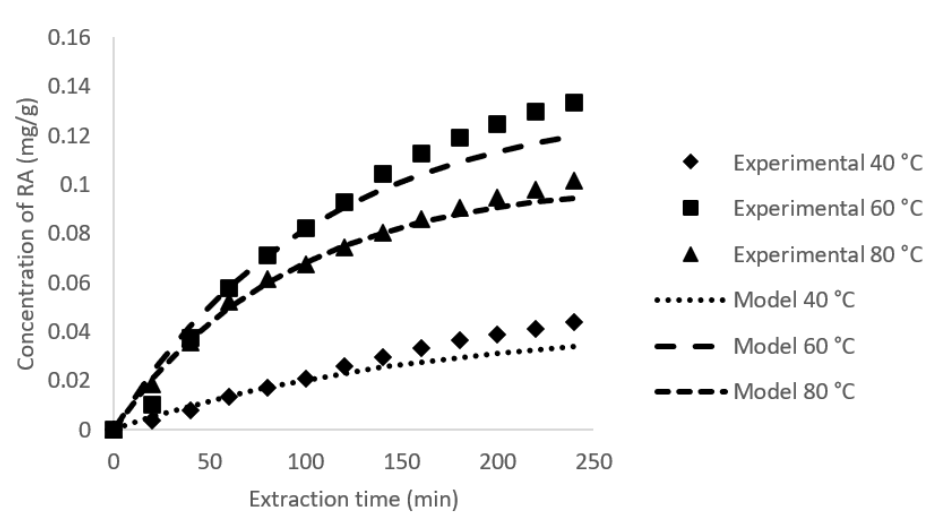
Figure 2. Interactions between RA molecules.

3.3. Rate of RA Extraction and Its Mass Transfer Coefficient

The rate of RA extraction and its mass transfer coefficient were evaluated at temperatures of 40 °C to 80 °C and pressures ranging from 10 to 30 MPa. Table 4 shows the mass transfer coefficient and extraction rate of RA using the Patricelli [68] model. Based on the low percentage value of AARD (<16%), the results demonstrate that the model matches the experimental data significantly. The fastest extraction rate of RA in the ethanol-assisted SCCO₂ system was 0.0061 mg/g min⁻¹ at 80 °C and 10 MPa, according to Table 4. Furthermore, the maximum equilibrium yield of RA was produced under the same conditions, which was approximately 0.9314 mg/g. As shown in the same table, the concentration of RA was higher during the washing phase than during the diffusion phase. During the washing phase, reduced mean particle size may have contributed to the quick dissolving of RA from the fractured cell walls into the solvent. As the extraction advanced to the diffusion phase, the extraction rate declined and grew slower. The washing phase has a larger mass transfer coefficient than the diffusion phase ($k_w > k_d$), which could explain this phenomenon. Furthermore, the model aligned well with experimental data, with R² values greater than 0.9652 for each extraction condition at constant pressures ranging from 10 to 30 MPa, as shown in Figures 3–5, respectively.

Table 4. Mass transfer coefficient and extraction rate of RA in ethanol-assisted SCCO₂ system using Patricelli model.

T (°C)	P (MPa)	Mass Transfer Coefficient (min ⁻¹)		RA (mg/g)		Extraction Rate (mg/g min ⁻¹)	Equilibrium RA (mg/g)	AARD (%)	R ²
		k_w	k_d	C_w	C_d				
40	10	0.0147	0.0135	0.0683	0.0522	0.0017	0.1205	3.6219	0.9907
60	10	0.0321	0.0127	0.1545	0.0606	0.0057	0.2151	1.7715	0.9960
80	10	0.0094	0.0093	1.3453	0.9914	0.0218	2.3367	4.5450	0.9652
40	20	0.0062	0.0063	0.0257	0.0180	0.0003	0.0437	14.7454	0.9930
60	20	0.0095	0.0095	0.0709	0.0625	0.0013	0.1334	14.9458	0.9957
80	20	0.0112	0.0111	0.0523	0.0493	0.0011	0.1016	3.3129	0.9979
40	30	0.0151	0.0102	0.0808	0.0460	0.0017	0.1268	3.5445	0.9963
60	30	0.0108	0.0108	0.1132	0.0552	0.0018	0.1684	8.1098	0.9974
80	30	0.0104	0.0104	0.0915	0.0491	0.0015	0.1406	6.2773	0.9963

**Figure 3.** Extraction curve of RA extract from OS at constant pressure of 10 MPa.**Figure 4.** Extraction curve of RA extract from OS at constant pressure of 20 MPa.

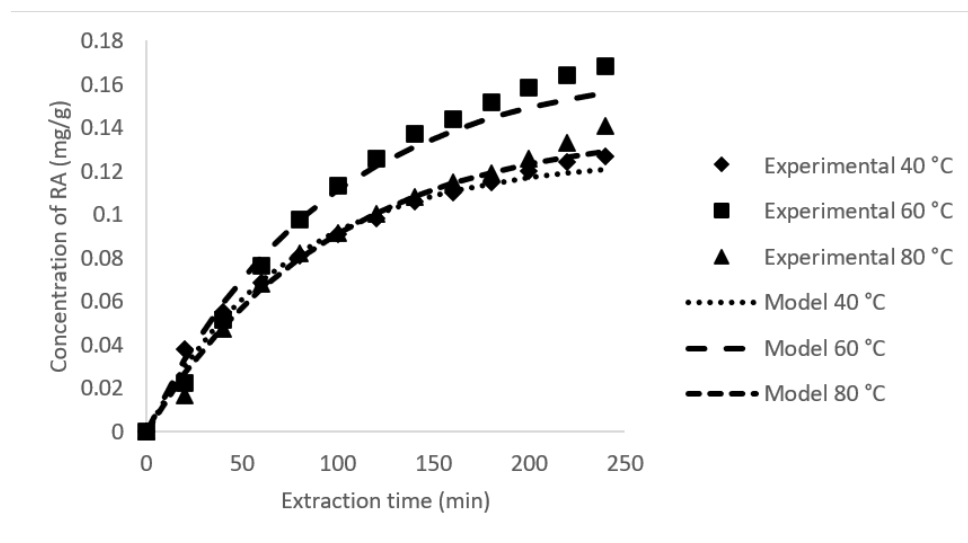


Figure 5. Extraction curve of RA extract from OS at constant pressure of 30 MPa.

4. Conclusions

In conclusion, the solubility of RA from OS leaves in ethanol-assisted SCCO₂ extraction range from 0.056 to 2.004 mg/L solvent at temperatures ranging from 40 to 80 °C and pressures ranging from 10 to 30 MPa. At temperatures ranging from 40 to 80 °C and pressures ranging from 10 to 30 MPa, the solubility of RA in ethanol-assisted SCCO₂ is the lowest when compared to other bioactive solutes from OS, viz. sinensetin, and isosinensetin. In the SCCO₂ system, the solute–solvent interaction has a major impact on the solute’s solubility. The hydrogen bonds produced between the RA molecules cause a strong solute–solvent interaction, causing the solvent to face steric hindrance in dissolving the solute. In this work, the density-based semi-empirical models used revealed a high correlation of RA solubility data with less than 10% AARD. Furthermore, using the Patricelli model, the extraction rate of RA in the ethanol-assisted SCCO₂ system was correctly determined in the range of 0.0003 to 0.0218 mg/g min⁻¹ in 40 to 80 °C and 10 to 30 MPa extraction conditions. Therefore, the information reported in this study can be used for further research and scaling up to extract RA via SCCO₂ extraction.

Author Contributions: Conceptualization, M.A.C.Y.; methodology, A.H.A.A.; software, N.R.P.; validation, M.A.A.; writing—original draft preparation, A.H.A.A.; writing—review and editing, N.F.M.I.; visualization, Z.I.; supervision, M.A.C.Y. and H.M. All authors have read and agreed to the published version of the manuscript.

Funding: This research was funded by the UTM Prototype Research Grant, with vote number Q.J130000.2851.00L35 from Universiti Teknologi Malaysia and Prototype Research Grant Scheme, vote number: R.J130000.7851.4L912 (PRGS/1/2020/TK02/UTM/02/1) from Ministry of Higher Education for financial support. The APC was funded by Universiti Malaysia Sabah.

Institutional Review Board Statement: Not applicable.

Informed Consent Statement: Not applicable.

Data Availability Statement: The data presented in this study are available on request from the corresponding author.

Acknowledgments: The authors would like to acknowledge the Centre of Lipids Engineering and Applied Research (CLEAR), UTM for the facilities provided, especially the supercritical carbon dioxide extraction unit. The authors would want to express their gratitude to Universiti Malaysia Sabah for providing financial assistance for APC.

Conflicts of Interest: The authors declare no conflict of interest.

References

1. Kamaruddin, M.J.; Hamid, S.R.A.; Othman, S.I.A.; Alam, M.N.H.Z.; Zaini, M.A.A.; Zakaria, Z.Y. The effects of conventional and microwave heating techniques on extraction yield of *Orthosiphon stamineus* leaves. *Chem. Eng. Trans.* **2018**, *63*, 601–606.
2. Himani, B.; Seema, B.; Bhole, N.; Mayank, Y.; Vinod, S.; Mamta, S. Misai kuching: A glimpse of maestro. *Int. J. Pharmaceut. Sci. Rev. Res.* **2013**, *22*, 55–59.
3. Aziz, A.H.A.; Yunus, M.A.C.; Yian, L.N.; Idham, Z.; Rithwan, F.; Hadzri, H.M.; Mustapha, A.N. Enhancement and optimization of sinensetin extract from *Orthosiphon stamineus* using supercritical carbon dioxide extraction. *Malays. J. Anal. Sci.* **2018**, *22*, 867–876.
4. Al-Suede, F.S.R.; Khadeer Ahamed, M.B.; Abdul Majid, A.S.; Baharetha, H.M.; Hassan, L.E.A.; Kadir, M.O.A.; Nassar, Z.D.; Abdul Majid, A.M.S. Optimization of Cat's Whiskers Tea (*Orthosiphon stamineus*) Using Supercritical Carbon Dioxide and Selective Chemotherapeutic Potential against Prostate Cancer Cells. *Evid.-Based Complem. Altern. Med.* **2014**, *2014*, 396016. [[CrossRef](#)]
5. Ghedira, K.; Goetz, P. *Orthosiphon stamineus* Benth.: *Orthosiphon* (Lamiaceae). *Phytothérapie* **2015**, *13*, 39–44. [[CrossRef](#)]
6. Hsu, C.-L.; Hong, B.-H.; Yu, Y.-S.; Yen, G.-C. Antioxidant and anti-inflammatory effects of *Orthosiphon aristatus* and its bioactive compounds. *J. Agric. Food Chem.* **2010**, *58*, 2150–2156. [[CrossRef](#)]
7. Adnyana, I.K.; Setiawan, F.; Insanu, M. From Ethnopharmacology to Clinical Study of *Orthosiphon Stamineus* Benth. *Int. J. Pharm. Pharm. Sci.* **2013**, *5*, 66–73.
8. Cher, H.L.; Lee, S.C.; Chew, T.L.; Ramlan, A. Optimization and Kinetic Modeling of Rosmarinic Acid Extraction from *Orthosiphon stamineus*. *Curr. Bioact. Comp.* **2014**, *10*, 271–285.
9. Abd Razak, N.; Yeap, S.K.; Alitheen, N.B.; Ho, W.Y.; Yong, C.Y.; Tan, S.W.; Tan, W.S.; Long, K. Eupatorin Suppressed Tumor Progression and Enhanced Immunity in a 4T1 Murine Breast Cancer Model. *Integr. Cancer Ther.* **2020**, *19*, 153473542093562. [[CrossRef](#)]
10. Al-Dulaimi, D.W.; Shah Abdul Majid, A.; Baharetha, M.H.; Ahamed, M.B.K.; Faisal, S.F.; Al Zarzour, R.H.; Ein Oon, C.; Abdul Majid, A.M.S.; Ahmed Hassan, L.E. Anticlastogenic, antimutagenic, and cytoprotective properties of *Orthosiphon stamineus* ethanolic leaves extract. *Drug Chem. Toxicol.* **2022**, *45*, 641–650. [[CrossRef](#)]
11. Pauzi, N.; Mohd, K.S.; Abdul Halim, N.H.; Ismail, Z. *Orthosiphon stamineus* Extracts Inhibits Proliferation and Induces Apoptosis in Uterine Fibroid Cells. *Asian Pac. J. Cancer Prev.* **2018**, *19*, 2737–2744. [[PubMed](#)]
12. Basheer, M.K.A.; Majid, A.M.S.A. Medicinal potentials of *Orthosiphon stamineus* Benth. *Webmedcentr. Cancer* **2010**, *1*, WMC001361.
13. Othman, N.F.; Ya'acob, M.E.; Abdul-Rahim, A.S.; Hizam, H.; Farid, M.M.; Abd Aziz, S. Inculcating herbal plots as effective cooling mechanism in urban planning. *Acta Horticult.* **2017**, *1152*, 235–242. [[CrossRef](#)]
14. Sik, B.; Hanczné, E.L.; Kapcsándi, V.; Ajtóny, Z. Conventional and nonconventional extraction techniques for optimal extraction processes of rosmarinic acid from six Lamiaceae plants as determined by HPLC-DAD measurement. *J. Pharmaceut. Biomed. Anal.* **2020**, *184*, 113173. [[CrossRef](#)]
15. Soraki, R.K.; Gerami, M.; Ramezani, M. Effect of graphene / metal nanocomposites on the key genes involved in rosmarinic acid biosynthesis pathway and its accumulation in *Melissa officinalis*. *BMC Plant Biol.* **2021**, *21*, 260. [[CrossRef](#)]
16. Jurić, T.; Mičić, N.; Potkonjak, A.; Milanov, D.; Dodić, J.; Trivunović, Z.; Popović, B.M. The evaluation of phenolic content, in vitro antioxidant and antibacterial activity of *Mentha piperita* extracts obtained by natural deep eutectic solvents. *Food Chem.* **2021**, *362*, 130226. [[CrossRef](#)] [[PubMed](#)]
17. Vasileva, L.V.; Savova, M.S.; Tews, D.; Wabitsch, M.; Georgiev, M.I. Rosmarinic acid attenuates obesity and obesity-related inflammation in human adipocytes. *Food Chem. Toxicol.* **2021**, *149*, 112002. [[CrossRef](#)]
18. Akowuah, G.A.; Zhari, I. Effect of Extraction Temperature on Stability of Major Polyphenols and Antioxidant Activity of *Orthosiphon stamineus* Leaf. *J. Herbs Spices Med. Plants* **2010**, *16*, 160–166. [[CrossRef](#)]
19. Abdul Aziz, A.H.; Putra, N.R.; Kong, H.; Che Yunus, M.A. Supercritical Carbon Dioxide Extraction of Sinensetin, Isosinensetin, and Rosmarinic Acid from *Orthosiphon stamineus* Leaves: Optimization and Modeling. *Arab. J. Sci. Eng.* **2020**, *45*, 7467–7476. [[CrossRef](#)]
20. Bernatoniene, J.; Cizauskaite, U.; Ivanauskas, L.; Jakstas, V.; Kalveniene, Z.; Kopustinskiene, D.M. Novel approaches to optimize extraction processes of ursolic, oleanolic and rosmarinic acids from *Rosmarinus officinalis* leaves. *Ind. Crops Prod.* **2016**, *84*, 72–79. [[CrossRef](#)]
21. Anwar, S.; Shamsi, A.; Shahbaaz, M.; Queen, A.; Khan, P.; Hasan, G.M.; Islam, A.; Alajmi, M.F.; Hussain, A.; Ahmad, F.; et al. Rosmarinic Acid Exhibits Anticancer Effects via MARK4 Inhibition. *Sci. Rep.* **2020**, *10*, 10300. [[CrossRef](#)] [[PubMed](#)]
22. Nguyen, H.C.; Nguyen, H.N.T.; Huang, M.-Y.; Lin, K.-H.; Pham, D.-C.; Tran, Y.B.; Su, C.-H. Optimization of aqueous enzyme-assisted extraction of rosmarinic acid from rosemary (*Rosmarinus officinalis* L.) leaves and the antioxidant activity of the extract. *J. Food Process. Preserv.* **2021**, *45*, e15221. [[CrossRef](#)]
23. Shekarchi, M.; Hajimehdipoor, H.; Saeidnia, S.; Gohari, A.; Hamedani, M. Comparative study of rosmarinic acid content in some plants of Labiatae family. *Pharm. Mag.* **2012**, *8*, 37–41.
24. Razboršek, M.I. Stability studies on trans-rosmarinic acid and GC-MS analysis of its degradation product. *J. Pharmaceut. Biomed. Anal.* **2011**, *55*, 1010–1016. [[CrossRef](#)]
25. Ramli, W.N.D.; Yunus, M.A.C.; Yian, L.N.; Idham, Z.; Aziz, A.H.A.; Aris, N.A.; Putra, N.R.; Sham, S.K. Extraction of squalene from *Aquilaria malaccensis* leaves using different extraction methods. *Mal. J. Anal. Sci.* **2018**, *22*, 973–983.

26. Priyadarsani, S.; Patel, A.S.; Kar, A.; Dash, S. Process optimization for the supercritical carbon dioxide extraction of lycopene from ripe grapefruit (*Citrus paradisi*) endocarp. *Sci. Rep.* **2021**, *11*, 10273. [[CrossRef](#)]
27. Putra, N.R.; Rizkiyah, D.N.; Zaini, A.S.; Machmudah, S.; Yunus, M.A.C. Solubility of catechin and epicatechin from *Arachis Hypogaea* skins wastes by using supercritical carbon dioxide-ethanol and its optimization. *J. Food Measur. Charact.* **2021**, *15*, 2031–2038. [[CrossRef](#)]
28. Abdul Aziz, A.H.; Putra, N.R.; Nian Yian, L.; Mohd Rasidek, N.A.; Che Yunus, M.A. Parametric and kinetic study of supercritical carbon dioxide extraction on sinensetin from *Orthosiphon stamineus* Benth. leaves. *Separ. Sci. Technol.* **2021**, *57*, 444–453. [[CrossRef](#)]
29. Idham, Z.; Putra, N.R.; Aziz, A.H.A.; Zaini, A.S.; Rasidek, N.A.M.; Mili, N.; Yunus, M.A.C. Improvement of extraction and stability of anthocyanins, the natural red pigment from roselle calyces using supercritical carbon dioxide extraction. *J. CO₂ Utiliz.* **2022**, *56*, 101839. [[CrossRef](#)]
30. Song, E.; Choi, J.; Gwon, H.; Lee, K.-Y.; Choi, S.-G.; Atiqal Islam, M.; Chun, J.; Hwang, J. Phytochemical profile and antioxidant activity of *Dracocephalum moldavica* L. seed extracts using different extraction methods. *Food Chem.* **2021**, *350*, 128531. [[CrossRef](#)]
31. Bakota, E.L.; Winkler-Moser, J.K.; Berhow, M.A.; Eller, F.J.; Vaughn, S.F. Antioxidant Activity and Sensory Evaluation of a Rosmarinic Acid-Enriched Extract of *Salvia officinalis*. *J. Food Sci.* **2015**, *80*, C711–C717. [[CrossRef](#)] [[PubMed](#)]
32. Lefebvre, T.; Destandau, E.; Lesellier, E. Sequential extraction of carnosic acid, rosmarinic acid and pigments (carotenoids and chlorophylls) from Rosemary by online supercritical fluid extraction-supercritical fluid chromatography. *J. Chromatogr. A* **2021**, *1639*, 461709. [[CrossRef](#)]
33. Putra, N.R.; Rizkiyah, D.N.; Abdul Aziz, A.H.; Machmudah, S.; Jumakir, J.; Waluyo, W.; Che Yunus, M.A. Procyanidin and proanthocyanidin extraction from *Arachis hypogaea* skins by using supercritical carbon dioxide: Optimization and modeling. *J. Food Process. Preserv.* **2021**, *18*, e15689. [[CrossRef](#)]
34. Sato, T.; Ikeya, Y.; Adachi, S.-I.; Yagasaki, K.; Nihei, K.-I.; Itoh, N. Extraction of strawberry leaves with supercritical carbon dioxide and entrainers: Antioxidant capacity, total phenolic content, and inhibitory effect on uric acid production of the extract. *Food Bioprod. Process.* **2019**, *117*, 160–169. [[CrossRef](#)]
35. Reddy, V.; Saharay, M. Solubility of Caffeine in Supercritical CO₂: A Molecular Dynamics Simulation Study. *J. Phys. Chem. B* **2019**, *123*, 9685–9691. [[CrossRef](#)] [[PubMed](#)]
36. Lemert, R.M.; Johnston, K.P. Solubilities and selectivities in supercritical fluid mixtures near critical end points. *Fluid Phase Equilib.* **1990**, *59*, 31–55. [[CrossRef](#)]
37. Huang, Z.; Chiew, Y.C.; Lu, W.-D.; Kawi, S. Solubility of aspirin in supercritical carbon dioxide/alcohol mixtures. *Fluid Phase Equilib.* **2005**, *237*, 9–15. [[CrossRef](#)]
38. Bitencourt, R.G.; Filho, W.A.R.; Paula, J.T.; Garmus, T.T.; Cabral, F.A. Solubility of γ -oryzanol in supercritical carbon dioxide and extraction from rice bran. *J. Supercrit. Fluids* **2016**, *107*, 196–200. [[CrossRef](#)]
39. Putra, N.R.; Aziz, A.H.A.; Idham, Z.; Rizkiyah, D.N.; Jumakir, J.; Mastaza, M.H.A.; Yunus, M.A.C. Kinetic modelling and extraction of *Orthosiphon stamineus* stems and leaves by SC-CO₂. *Malays. J. Fund. Appl. Sci.* **2020**, *16*, 602–608.
40. Putra, N.R.; Rizkiyah, D.N.; Abdul Aziz, A.H.; Idham, Z.; Qomariyah, L.; Che Yunus, M.A. Extraction rate of Valuable Compounds from Peanut Skin Waste by Ethanol-Assisted Supercritical Carbon Dioxide: Modelling and Optimization. *Malays. J. Fund. Appl. Sci.* **2022**, *18*, 157–170. [[CrossRef](#)]
41. Sodeifian, G.; Alwi, R.S.; Razmimanesh, F.; Tamura, K. Solubility of Quetiapine hemifumarate (antipsychotic drug) in supercritical carbon dioxide: Experimental, modeling and Hansen solubility parameter application. *Fluid Phase Equilib.* **2021**, *537*, 113003. [[CrossRef](#)]
42. Antonie, P.; Pereira, C.G. Solubility of functional compounds in supercritical CO₂: Data evaluation and modelling. *J. Food Eng.* **2019**, *245*, 131–138. [[CrossRef](#)]
43. Putra, N.; Aziz, A.A.; Zaini, A.; Idham, Z.; Idrus, F.; Zullyadini, M.B.; Yunus, M.C. Optimization of Soybean Oil by Modified Supercritical Carbon Dioxide. *Int. J. Chem. Mol. Eng.* **2018**, *12*, 495–500.
44. Cheng, J.; Han, S.; Song, J.; Wang, W.; Jiao, Z. Solubility of Vitamin E Acetate in Supercritical Carbon Dioxide with Ethanol as Cosolvent. *J. Chem. Eng. Data* **2018**, *63*, 4248–4255. [[CrossRef](#)]
45. Mouahid, A.; Bombarda, I.; Claeys-Bruno, M.; Amat, S.; Myotte, E.; Nisteron, J.-P.; Crampon, C.; Badens, E. Supercritical CO₂ extraction of Moroccan argan (*Argania spinosa* L.) oil: Extraction kinetics and solubility determination. *J. CO₂ Utiliz.* **2021**, *46*, 101458. [[CrossRef](#)]
46. Hazaveie, S.M.; Sodeifian, G.; Sajadian, S.A. Measurement and thermodynamic modeling of solubility of Tamsulosin drug (anti cancer and anti-prostatic tumor activity) in supercritical carbon dioxide. *J. Supercrit. Fluids* **2020**, *163*, 104875. [[CrossRef](#)]
47. Rosales-García, T.; Rosete-Barreto, J.M.; Pimentel-Rodas, A.; Davila-Ortiz, G.; Galicia-Luna, L.A. Solubility of Squalene and Fatty Acids in Carbon Dioxide at Supercritical Conditions: Binary and Ternary Systems. *J. Chem. Eng. Data* **2017**, *63*, 69–76. [[CrossRef](#)]
48. Guo, L.; Qu, M.; Jin, J.; Meng, H. Solubility of cinnamic acid in supercritical carbon dioxide and subcritical 1,1,1,2-tetrafluoroethane: Experimental data and modelling. *Fluid Phase Equilib.* **2019**, *480*, 66–80. [[CrossRef](#)]
49. Chrastil, J. Solubility of solids and liquids in supercritical gases. *J. Phys. Chem.* **1982**, *86*, 3016–3021. [[CrossRef](#)]
50. Adachi, Y.; Lu, B.C.Y. Supercritical fluid extraction with carbon dioxide and ethylene. *Fluid Phase Equilib.* **1983**, *14*, 147–156. [[CrossRef](#)]

51. Kumar, S.K.; Johnston, K.P. Modelling the solubility of solids in supercritical fluids with density as the independent variable. *J. Supercrit. Fluids* **1988**, *1*, 15–22. [[CrossRef](#)]
52. Sung, H.-D.; Shim, J.-J. Solubility of C. I. Disperse Red 60 and C. I. Disperse Blue 60 in Supercritical Carbon Dioxide. *J. Chem. Eng. Data* **1999**, *44*, 985–989. [[CrossRef](#)]
53. Méndez-Santiago, J.; Teja, A.S. The solubility of solids in supercritical fluids. *Fluid Phase Equilib.* **1999**, *158–160*, 501–510. [[CrossRef](#)]
54. Bartle, K.D.; Clifford, A.A.; Jafar, S.A.; Shilstone, G.F. Solubilities of Solids and Liquids of Low Volatility in Supercritical Carbon Dioxide. *J. Phys. Chem. Ref. Data* **1991**, *20*, 713–756. [[CrossRef](#)]
55. González, J.C.; Vieytes, M.R.; Botana, A.M.; Vieites, J.M.; Botana, L.M. Modified mass action law-based model to correlate the solubility of solids and liquids in entrained supercritical carbon dioxide. *J. Chromatogr. A* **2001**, *910*, 119–125. [[CrossRef](#)]
56. Sovová, H. Solubility of ferulic acid in supercritical carbon dioxide with ethanol as cosolvent. *J. Chem. Eng. Data* **2001**, *46*, 1255–1257. [[CrossRef](#)]
57. Tang, Z.; Jin, J.-s.; Zhang, Z.-t.; Yu, X.-y.; Xu, J.-N. Solubility of 3,5-Dinitrobenzoic Acid in Supercritical Carbon Dioxide with Cosolvent at Temperatures from (308 to 328) K and Pressures from (10.0 to 21.0) MPa. *J. Chem. Eng. Data* **2010**, *55*, 3834–3841. [[CrossRef](#)]
58. Saucéau, M.; Letourneau, J.-J.; Richon, D.; Fages, J. Enhanced density-based models for solid compound solubilities in supercritical carbon dioxide with cosolvents. *Fluid Phase Equilib.* **2003**, *208*, 99–113. [[CrossRef](#)]
59. Zhan, S.; Li, S.; Zhao, Q.; Wang, W.; Wang, J. Measurement and Correlation of Curcumin Solubility in Supercritical Carbon Dioxide. *J. Chem. Eng. Data* **2017**, *62*, 1257–1263. [[CrossRef](#)]
60. Jin, J.-S.; Wang, Y.-W.; Zhang, H.-F.; Fan, X.; Wu, H. Solubility of 4-Hydroxybenzaldehyde in Supercritical Carbon Dioxide with and without Cosolvents. *J. Chem. Eng. Data* **2014**, *59*, 1521–1527. [[CrossRef](#)]
61. Wei, M.-C.; Xiao, J.; Yang, Y.-C. Extraction of α -humulene-enriched oil from clove using ultrasound-assisted supercritical carbon dioxide extraction and studies of its fictitious solubility. *Food Chem.* **2016**, *210*, 172–181. [[CrossRef](#)] [[PubMed](#)]
62. Jia, J.-F.; Zabihi, F.; Gao, Y.-H.; Zhao, Y.-P. Solubility of Glycyrrhizin in Supercritical Carbon Dioxide with and without Cosolvent. *J. Chem. Eng. Data* **2015**, *60*, 1744–1749. [[CrossRef](#)]
63. Soetaredjo, F.E.; Ismadji, S.; Yuliana Liauw, M.; Angkawijaya, A.E.; Ju, Y.-H. Catechin sublimation pressure and solubility in supercritical carbon dioxide. *Fluid Phase Equilib.* **2013**, *358*, 220–225. [[CrossRef](#)]
64. Abdul Aziz, A.H.; Putra, N.R.; Zaini, A.S.; Idham, Z.; Ahmad, M.Z.; Che Yunus, M.A. Solubility of sinensetin and isosinensetin from Cat's Whiskers (*Orthosiphon stamineus*) leaves in ethanol-assisted supercritical carbon dioxide extraction: Experimental and modeling. *Chem. Papers* **2021**, *75*, 6557–6563. [[CrossRef](#)]
65. Putra, N.R.; Rizkiyah, D.N.; Abdul Aziz, A.H.; Idham, Z.; Jumakir, J.; Waluyo, W.; Che Yunus, M.A. Application of Drying Model to Determine Extraction Behaviours on Peanut Skin Oil Recovery by Supercritical Carbon Dioxide-Ethanol. *Malays. J. Fund. Appl. Sci.* **2021**, *17*, 114–127. [[CrossRef](#)]
66. Ruslan, M.S.H.; Idham, Z.; Nian Yian, L.; Ahmad Zaini, M.A.; Che Yunus, M.A. Effect of operating conditions on catechin extraction from betel nuts using supercritical CO₂-methanol extraction. *Separ. Sci. Technol.* **2018**, *53*, 662–670. [[CrossRef](#)]
67. Del Valle, J.M.; Aguilera, J.M. An improved equation for predicting the solubility of vegetable oils in supercritical carbon dioxide. *Ind. Eng. Chem. Res.* **1988**, *27*, 1551–1553. [[CrossRef](#)]
68. Patricelli, A.; Assogna, A.; Casalaina, A.; Emmi, E.; Sodini, G. Fattoriche influenzano l'estrazione dei lipidi da semi decorticati di girasole. *La Revista Italiana Delle Sostanze Grasse* **1979**, *56*, 151–154.
69. Paviani, L.C.; Dariva, C.; Marcucci, M.C.; Cabral, F.A. Supercritical carbon dioxide selectivity to fractionate phenolic compounds from the dry ethanolic extract of propolis. *J. Food Process Eng.* **2010**, *33*, 15–27. [[CrossRef](#)]